Multivalent Ion Distribution around a Cylindrical Polyion: Contribution of Polarization Effects Due to Difference between Dielectric Properties of the Macromolecule's Interior and the Aqueous Solvent

Sergei Gavryushov* and Piotr Zielenkiewicz

Institute of Biochemistry and Biophysics, Polish Academy of Sciences, Pawinskiego 5a, 02-106 Warszawa, Poland

Received: July 15, 1996; In Final Form: October 7, 1996[⊗]

The Bogolyubov−Born−Green−Yvon (BBGY) equations have been applied to study ionic and mean electrostatic potential distributions around an extremely simplified model of the DNA at low ionic concentrations. Dielectric discontinuities have been taken into account. Results are compared with those obtained in classical Poisson−Boltzmann calculations which neglect the effect of ion−image charge interactions and interionic correlations. It is shown that concentration profiles of divalent counterions are sensitive to the structural elements of the solvent, i.e., the location of the dielectric discontinuities, whereas this effect is negligible for monovalent ions. The numerical method used can be applied to calculate ionic distributions around macromolecules of arbitrary shape placed into dilute solution of multivalent electrolyte.

1. Introduction

For the past 20 years the computation of ionic distributions around highly charged biopolymers has been a subject of continuous interest. Several approaches were proposed to solve this problem; they vary widely with respect to simplification of macromolecule−ion−water interactions. First theories for treating nonspecific salt effects and DNA−ligand binding were originally based on counterion condensation, or limiting law (infinite length polyelectrolyte at infinite salt dilution) theories.[1−3] If one simplifies a DNA structure to an infinitely long, uniformly charged cylinder, it is possible to compute the average cylindrically symmetric ionic distributions through the numerical solution of hypernetted chain (HNC) equation[4] or by the Monte Carlo (MC) technique.[4,5] Both methods are quite exact in the frame of Coulombic electrostatic interactions with macroscopic permittivity of water.

Another approach is to solve numerically the Poisson−Boltzmann (PB) equation, which can be done for enough realistic structural models of DNA.[6] The PB model includes the difference in polarizabilities of water and interior of the macromolecule (which is assumed to be much lower) but ignores short-range non-Coulombic repulsion between ions (i.e., considers ions as point charges), which reduces the range of salt concentrations over which the distribution can be obtained to dilute solutions. In the case of equal dielectric constants inside and outside DNA, the PB equation was checked by the comparison with theoretically more exact HNC equation and MC simulations for the simplest model of a uniformly charged cylinder.[4]

Recently, a new method of computation of ionic distributions around charged macromolecules has been proposed.[7] The method is based on the potential of mean force (PMF) approach, and it can be used for arbitrarily complex charged biomolecular structures. It is important to note that the PMF approach neglects higher order polarization effects due to differences between dielectric properties of DNA interior and the aqueous solvent.[8] This assumption seems to be reasonable at high concentrations of ions but it is inadequate at low ionic concentrations where the model with macroscopic dielectric constants can be used. At present the PB equation is the only method that allows study of salt-dependence effects on the free energy, entropy, and enthalpy of a polyelectrolyte if we want to take into account both the geometry of macromolecules and a difference between dielectric constants of the macromolecule and solvent. An advantage of the PB model is that the contribution of these parameters is significant to the salt dependence of free binding energy.[9]

The present work analyzes ionic distributions around the cylindrical polyion at low ionic concentrations (∼0.1 M) on the basis of the BBGY equations[10]—an exact formalism which can be applied to the electrical double layer. Being supplemented by a suitable closure approximation, these equations lead to a more advanced theory than the PB approach. Many more detailed effects can be incorporated into the theory, in particular, short-range nonelectrostatic interactions between ions and polarization effect due to dielectric discontinuities of the solvent. The last effect is also known as the electrostatic image effect and is ignored by the PB equation.[10] We use the restricted primitive model (RPM) of electrolyte for the description of short-range interactions between ions (i.e., ions are represented by hard spheres), although it is not obligatory for numerical implementation. There are other theories of electrical double layer which incorporate image effects—the Modified Poisson−Boltzmann (MPB) theory[10] and the anisotropic hypernetted chain (anisotropic HNC) theory.[11,12] The MPB theory was initiated with the work of Bell and Levine,[13,14] and it has been one of the most successful formal statistical mechanical theories. The MPB equation was formulated for the planar, spherical, and cylindrical geometries.[15−17] These applications were designed for analytical solutions of the involved electrostatic boundary value problems, which can be only done for dilute McMillan−Mayer level electrolytes and simplest geometries.[10] The image effect could only be explicitly included for the planar geometry.[15,18] The basis of the MBP theory is the Kirkwood hierarchy of equations together with linearized Loeb's closure ("weak ion−ion coupling").[10] In the present research we apply the same approximation to the BBGY hierarchy of equations and replace analytical solutions of involved electrostatic bound-

* Author to whom correspondence should be addressed. Telephone: 48 2 6584703. Fax: 48 39 121623. E-mail: serg@ibbrain.ibb.waw.pl.

[⊗] Abstract published in *Advance ACS Abstracts,* December 15, 1996.

S1089-5647(96)02101-3 CCC: $14.00

ary value problems by their numerical implementation. It is important to note that although equations given by the BBGY and Kirkwood hierarchies together with Loeb's closure are close to each other, they are different for a model with finite-size ions. The equations coincide in the limiting case of pointlike ions as a set of partial differential equations, which distinguishes these theories from the anisotropic HNC theory based on the integral Ornstein−Zernike equation.

The present paper is pointed to study the effect of permittivity discontinuities for the simplest model of the infinitely long, uniformly charged cylinder. Previous applications of the HNC[4] and the MPB[19] theories for this model were based on the assumption that this effect is negligible. (Numerous applications of the PB equation to the DNA are not considered as the last approach is too rough to describe the effect, although the function of permittivity is included into the PB equation.) Despite the mentioned assumption about the weakness of the dielectric discontinuities effect, there is evidence that it is important for understanding colloidal aggregation in the presence of divalent ions.[20] This effect is also responsible for a salting-out phenomenon on solubility of proteins.[21]

In order to study the effect of dielectric discontinuities, original boundary value problems involved in the BBGY approach were programmed numerically and the algorithm was tested on models of weakly charged and uncharged cylinders where analytical solutions are known. Such dielectric effects as the charge−cavity interionic interactions[22] and the dielectric saturation effects were not considered although they can be incorporated into the equations.

This article is organized as follows. In the next section the method of calculations is explained. In section 3 some details of numerical implementation of the method are described. Comparison of numerical results with MC simulations taken from ref 19 is also given. In section 4 we compare results for uniformly charged cylinder with the PB approach at various dielectric constants and ionic concentrations of 1:1 and 2:1 electrolytes.

2. Theory

The BBGY hierarchy together with linearized Loeb's closure gives the following equations for distribution of ions of species α, represented by hard spheres of diameter d:[10]

$$\ln g_\alpha(\mathbf{r}) = \ln \xi_\alpha(\mathbf{r}) - \beta q_\alpha \psi(\mathbf{r}) - \beta q_\alpha [\eta_\alpha(\mathbf{r}) - \eta_\alpha(\infty)] \quad (1)$$

where $\beta = 1/kT$, q_α is the charge of an ion, $\psi(\mathbf{r})$ is the mean electrostatic potential, $-kT \ln \xi_\alpha(\mathbf{r})$ is the work required to insert an uncharged ion at point $\mathbf{r}$ and $\eta_\alpha(\mathbf{r})$ satisfies an equation

$$\nabla_2 \eta_\alpha(\mathbf{r}_2) = \lim_{\mathbf{r}_1 \to \mathbf{r}_2} \nabla_1 [\phi_\alpha(\mathbf{r}_1,\mathbf{r}_2) - q_\alpha u^c(r_{12})] \quad (2)$$

where $u^c(r_{12})$ is Coulombic self-potential of the ion and $\phi_\alpha(\mathbf{r}_1,\mathbf{r}_2)$ is the fluctuation potential. The last satisfies the exact equations for the RPM:

$$\nabla_1^2 \phi_\alpha(\mathbf{r}_1,\mathbf{r}_2) = 0 \quad (3.1)$$

(inside the macromolecule's interior and a shell of thickness $d/2$ surrounding the surface of the macromolecule)

$$\nabla_1^2 \phi_\alpha(\mathbf{r}_1,\mathbf{r}_2) = -\nabla_1^2 \psi(\mathbf{r}_1) - \frac{4\pi}{\epsilon_w} q_\alpha \delta(\mathbf{r}_1 - \mathbf{r}_2) \quad (3.2)$$

(outside the macromolecule and the "shell $d/2$", $r_{12} < d$)

$$\nabla_1^2 \phi_\alpha(\mathbf{r}_1,\mathbf{r}_2) = k^2(\mathbf{r}_1) \phi_\alpha(\mathbf{r}_1,\mathbf{r}_2) \quad (3.3)$$

(outside the macromolecule and the "shell $d/2$", $r_{12} > d$) where

$$k^2(\mathbf{r}) = 4\pi\beta \sum_\gamma \frac{n_\gamma^0 g_\gamma(\mathbf{r}) q_\gamma^2}{\epsilon_w}$$

Equations 3.1−3.3 subject to the boundary conditions on the surface of the macromolecule

$$\begin{aligned} \phi_\alpha|_{\text{inside}} &= \phi_\alpha|_{\text{outside}} \\ \epsilon \frac{\partial \phi_\alpha}{\partial n}\Big|_{\text{inside}} &= \epsilon_w \frac{\partial \phi_\alpha}{\partial n}\Big|_{\text{outside}} \end{aligned} \quad (4)$$

where ϵ and ϵ_w are dielectric constants of macromolecule's interior and water, respectively. The mean electrostatic potential $\psi(\mathbf{r})$ from eq 1 satisfies the Poisson equation

$$\begin{aligned} \nabla^2 \psi(\mathbf{r}) &= -\frac{4\pi}{\epsilon} \rho_0(\mathbf{r}) \qquad \text{inside the macromolecule} \\ \nabla^2 \psi(\mathbf{r}) &= -\frac{4\pi}{\epsilon_w} \sum_\gamma q_\gamma n_\gamma^0 g_\gamma(\mathbf{r}) \qquad \text{outside the macromolecule} \end{aligned} \quad (5)$$

where ρ_0 is the charge density of the macromolecule. The boundary conditions are

$$\begin{aligned} \psi|_{\text{inside}} &= \psi|_{\text{outside}} \\ \epsilon \frac{\partial \psi}{\partial n}\Big|_{\text{inside}} - \epsilon_w \frac{\partial \psi}{\partial n}\Big|_{\text{outside}} &= 4\pi\sigma_0 \end{aligned} \quad (6)$$

where σ_0 is the surface charge density of the macromolecule. The specification of the term $\ln \xi_\alpha(\mathbf{r})$ completes the set of equations. This so-called exclusion volume term may be approximated by[14]

$$-\int_{V_\alpha} \sum_\gamma (n_\gamma(\mathbf{r}) - n_\gamma^0)\, dV$$

where $n_\gamma(\mathbf{r}) = n_\gamma^0 g_\gamma(\mathbf{r})$ and n_γ^0 are the mean ionic concentration and the bulk ionic concentration, respectively, $V_\alpha = 4\pi d^3/3$ is the excluded volume of a small ion of diameter d. The numerical solution of the set of eqs 1−6 proceeds by inserting solution $\phi_\alpha(\mathbf{r}_1,\mathbf{r}_2)$ of eqs 3.1−3.3 into eq 1 and then into the Poisson equation (eq 5). The first step in such an algorithm is calculation of $\phi_\alpha^{(0)}(\mathbf{r}_1,\mathbf{r}_2)$. From $\phi^{(0)}$ one obtains $g_\alpha^{(0)}(\mathbf{r})$ through eq 1 and $\psi^{(0)}(\mathbf{r})$ through eq 5, which gives $\phi^{(1)}$ through eq 3 and so on. This procedure was applied for the weak-coupling theory for the point-ion model[10] which is a formulation of eqs 1−5 for the pointlike ions. The procedure should be continued to self-consistency.[10]

The main difficulty to solve eq 3 numerically follows from eqs 2 and 3.2 due to singularities in both of them. If an ordinary rectangular grid is used for the solution of elliptic partial differential eq 3, the magnitude of ϕ at the point of like-δ-function charge density is completely dependent on the grid spacing. We evaluate components of the gradient from eq 2 as, for example,

$$\frac{\partial}{\partial x} \eta_\alpha(\mathbf{r}_2) \approx \frac{1}{2\Delta X} [\phi_\alpha(\mathbf{r}_2 + \Delta\mathbf{x},\mathbf{r}_2) - \phi_\alpha(\mathbf{r}_2 - \Delta\mathbf{x},\mathbf{r}_2)]$$

The singularity is subtracted due to its symmetry and one can expect that the written difference does not essentially depend on the lattice spacing and mainly depends on boundary conditions. As follows from tests, a value of $\Delta\mathbf{x}$ may be equal

to the distance between grid points if the "diameter" of charge q_γ in eq 3.2 is equal to the lattice spacing (see below).

Equation 5 is a nonlinear elliptic partial differential equation. For a macromolecule of arbitrary shape and charge distribution it may be solved like the nonlinear PB equation.[6] In particular case of the infinitely long uniformly charged cylinder, the problem is reduced to an ordinary differential equation

$$\frac{1}{r}\frac{\mathrm{d}}{\mathrm{d}r}\left(r\frac{\mathrm{d}}{\mathrm{d}r}\psi(r)\right) = -\frac{4\pi}{\epsilon_\mathrm{w}}\sum_\gamma q_\gamma n_\gamma^0 \xi_\gamma(r)\, \mathrm{e}^{-\beta q_\gamma \psi(r) - \beta q_\gamma(\eta_\gamma(r)-\eta_\gamma(\infty))} \tag{7}$$

where $\xi_\gamma(r)$ denotes the exclusion volume term.

Equation 7 is solved subject to the two boundary conditions

$$\psi(R) = 0 \tag{8.1}$$

$$\left.\frac{\mathrm{d}\psi(r)}{\mathrm{d}r}\right|_{r=r_0} = -\frac{4\pi\sigma_0}{\epsilon_\mathrm{w}} \tag{8.2}$$

where r_0 is a radius of the cylinder and $R \gg r_0$. Boundary condition 8.1 can be also written for the cell model:[19]

$$\left.\frac{\mathrm{d}\psi(r)}{\mathrm{d}r}\right|_{r=R_\mathrm{c}} = 0 \tag{8.1.a}$$

Functions $\xi_\gamma(r)$ and $\eta_\gamma(r) - \eta_\gamma(\infty)$ result from numerical finite-difference solutions of 3-dimensional eq 3 for several points $\mathbf{r}_2$ lying with some step on radial line outside the cylinder. The mean potential $\psi(r)$, implicitly involved in eq 3, is taken from previous iteration. The calculated discrete values of $\xi_\gamma(r)$ and $\eta_\gamma(r) - \eta_\gamma(\infty)$ are interpolated by the cubic spline.

3. Model and Techniques

The set of eqs 1−4, 7, and 8 was implemented on the SGI Challenge L computer (R4400, 150 MHz). The algorithm was written in FORTRAN language. The eq 3 was programmed for finite difference method. The iterative relaxation process was repeated until the maximum absolute value of the change in successive iterations is less than 5×10^{-6}. A dense cubic lattice was used. The lattice was centred by each point $\mathbf{r}_2$ of charge $q_\alpha\delta(\mathbf{r}-\mathbf{r}_2)$ in eq 3.2. The shortest length of the lattice was from six to eight Debye−Huckel lengths of bulk electrolyte. The number of points was $119 \times 101 \times 101$ (the higher dimension corresponds to the radial direction), so even at the lowest ionic strength of the bulk electrolyte equal to 0.1 M, the spacing between lattice points was from 1.0 to 1.3 Å.

The finite difference implementation of the right-hand part of eq 3.2 required an accurate treatment. We used no charge distribution for the δ function. The charge $q_\alpha\delta(\mathbf{r}-\mathbf{r}_2)$ was assigned to the lattice node. Although such treatment seems to be rough, comparisons with known analytical solutions show that calculated gradients of $\eta(r)$ mainly depend on the boundary conditions and do not depend on the lattice spacing if the lattice is dense enough. The more advanced method of discretization of the dielectric discontinuity problem than used in ref 6 can be applied due to explicit expression of the normal vector on the surface of the cylinder. The method was used to increase accuracy of solution of eq 3 if the point $\mathbf{r}_2$ is situated close to the interface. This allowed the influence of dielectric boundary conditions on ϕ and, consequently, on $\eta(r)$ from eq 2 to be seen. If we consider, for instance, X axis, then boundary condition (4) can be written as

$$\epsilon_1\frac{\partial\phi^{(1)}}{\partial x} - \epsilon_2\frac{\partial\phi^{(2)}}{\partial x} = (\epsilon_2 - \epsilon_1)\frac{\partial\phi^{(1,2)}}{\partial\tau}\sqrt{1 - n_x^{\,2}}$$

TABLE 1: Testing η Calculations[a]

	$-\beta\mathrm{e}(\eta(r_2) - \eta(\infty))$	
r_2, Å	calculated	analytical
1. No Dielectric Discontinuities; $\epsilon = 80$		
10.4	−0.044	−0.045
11.4	−0.028	−0.030
12.5	−0.019	−0.021
13.5	−0.013	−0.016
14.6	−0.0094	−0.012
15.6	−0.0067	−0.0088
16.6	−0.0049	−0.0068
17.7	−0.0036	−0.0052
2. $\epsilon = 2$		
11.4	−0.86	−0.72
12.5	−0.34	−0.32
13.5	−0.19	−0.18
14.6	−0.12	−0.11
15.6	−0.075	−0.073
16.6	−0.051	−0.050
17.7	−0.035	−0.035
18.7	−0.025	−0.026

[a] Radius of cylinder is 10Å; the $119 \times 101 \times 101$ grid's spacing is 1.04 Å; the Debue−Huckel length $1/K$ is 13.7 Å.

where indexes 1 and 2 correspond to interior of the cylinder and surrounding medium (solvent), respectively; $\partial\phi^{(1,2)}/\partial\tau$ denotes the continuous tangential derivative of ϕ and n_X is the X-component of the normal vector. Expressing $\partial\phi^{(1,2)}/\partial\tau$ through partial derivatives of ϕ, we obtain

$$\epsilon_1\frac{\partial\phi^{(1)}}{\partial x} - \epsilon_2\frac{\partial\phi^{(2)}}{\partial x} = (\epsilon_2 - \epsilon_1)\left[\frac{\partial\phi^{(1,2)}}{\partial x}(n_x^{\,2} - 1) + \frac{\partial\phi^{(1,2)}}{\partial y}n_x n_y + \frac{\partial\phi^{(1,2)}}{\partial z}n_x n_z\right]$$

The last formula can be written in a discrete form for seven-point finite difference technique, which allows the unknown value of ϕ at the point of discontinuity of ϵ to be written. Discrete form of the second partial derivative of ϕ at each particular grid point is

$$\frac{\partial^2\phi}{\partial x^2} = \frac{1}{h}\left(\left.\frac{\partial\phi}{\partial x}\right|_{x+0} - \left.\frac{\partial\phi}{\partial x}\right|_{x-0}\right)$$

where h is the grid spacing. The chosen method of discretization was tested for a simplified form of eq 3:

$$\begin{aligned}\nabla_1^2\phi(\mathbf{r}_1,\mathbf{r}_2) &= 0 \qquad \text{(inside the cylinder)}\\ \nabla_1^2\phi(\mathbf{r}_1,\mathbf{r}_2) - K^2\phi(\mathbf{r}_1,\mathbf{r}_2) &= -\frac{4\pi}{\epsilon_\mathrm{w}}e\delta(\mathbf{r}_1 - \mathbf{r}_2) \qquad \text{(outside the cylinder)}\end{aligned} \tag{9}$$

where ϕ satisfies boundary conditions 4 and K is the inverse Debue−Huckel length of bulk electrolyte. Equation 9 is a linearized form of eq 3 in case of weak self-potential of the cylinder and pointlike ions (which cannot be applied to the model of highly charged DNA) and can be solved analytically, which allows the method to be tested. Results of comparison of calculated η function to the analytical data are given in Table 1 for the two cases $\epsilon = \epsilon_\mathrm{w} = 80$ and $\epsilon = 2$. The boundary conditions have been also tested, showing relative errors of finite difference equation less than 1% elsewhere for boundary grid points. Relative numerical errors of ϕ agree with analytical solutions to within 1% in case of absence of dielectric discontinuity and within a few percents in the case of $\epsilon = 2$ even if the point charge was situated very close to the cylinder surface. The gradient from eq 2 was calculated as

$$\frac{\partial}{\partial r}\eta(r_1) \approx \frac{1}{2h}[\phi(r_1+h,r_1) - \phi(r_1-h,r_1)]$$

where h is the spacing between lattice points. It is important to note that, in case of discontinuous dielectric medium, the calculations of η are not so accurate in the vicinity of the cylinder due to the difficulty of the gradient evaluation near the dielectric boundary. The error is up to 20% if the charge is one grid spacing away from the boundary, but decreases to several percents at longer distances.

Finally, the method has been tested on the data of MC simulations for DNA-like linear polyelectrolyte. The data were taken from ref 19, describing application of the MPB theory to the double layer around a highly uniformly charged cylinder of solvent permittivity and completed by MC simulations. We obtained the full numerical solution of eqs 1−3 and 7 for exactly the same model of 2:2 electrolyte corresponding to Figures 13 and 14 of this work. Our results shown in Figures 1 and 2, respectively, agree with data of simulations better than semi-analytical MPB approach[17] used in the referred paper. They are much closer to MC simulations than the ion distribution functions from the nonlinear PB equation which are also given in Figures 1 and 2. All physical parameters were the same as in the reference work. The 119 × 101 × 101 lattice was used to solve eq 3. The lattice's spacing was 1.25 Å for $c = 0.0125$ M (Figure 1) and 0.7 Å for $c = 0.05$ M (Figure 2). The convergence of the iteration process (7)-(3)-(1)-(7) - etc. was very fast—it was obtained after four loops (3)-(1)-(7), so as a change in calculated potential ψ from eq 7 became less than 1%. The initial $\eta(r)$ was taken from analytical solution of eq 9 for the cylinder.

We can assume that the better agreement of our results with the MC data might originate from simplifications necessarily used in analytical solutions of the boundary value problem 3 for $\phi(\mathbf{r}_1,\mathbf{r}_2)$ involved into the MPB theory.[17] Some discrepancy between BBGY and MPB results might come from a difference between eq 2 and its analogue in the Kirkwood hierarchy applied to the RPM.[10]

It should be noted that all the applications described in this paper were computationally very expensive despite the mentioned rapid convergence of the main cycle. A number of solutions of eq 3 at various $\mathbf{r}_2$ was typically about 30, thus the four iterations (3)-(1)-(7) required to obtain 120 solutions of eq 3 (four calculations of ordinary differential eq 7 took negligible time in comparison with eq 3). Time of calculation of eq 3 was about 10 min on the R4400 processor, so typical runs required about 20 h on the SGI system.

4. Results and Discussion

The set of equations 1−3 and 7 has been solved numerically as an iteration process for 1:1 and 1:2 electrolytes with various values of dielectric constants, ionic diameter and ionic concentration. The PB equation is also solved for these data to make comparison with the BBGY calculations. We took $r_{ion} = 2$ Å (for comparison also 1 Å), $\epsilon_w = 80$, $T = 298$ K. The model of DNA is represented by a hard cylinder of 8 Å radius with uniform dielectric constant of 2, 10, and 80. The surface charge density corresponds to linear lattice of negative charges placed 1.7 Å apart on the axis of the cylinder.[6] This model is close to the model from ref 19, used for the testing (see above). The model of isolated double layer is used, i.e., with the polyion at infinity dilution. Results for 1:1 electrolyte are given in Figure 3, results for 2:1 electrolyte are displayed in Figures 4−9 (counterions are divalent). Comparison of counterion distributions for 1:1 salt shows a good agreement of BBGY and PB equations for both cases of uniform permittivity and dielectric

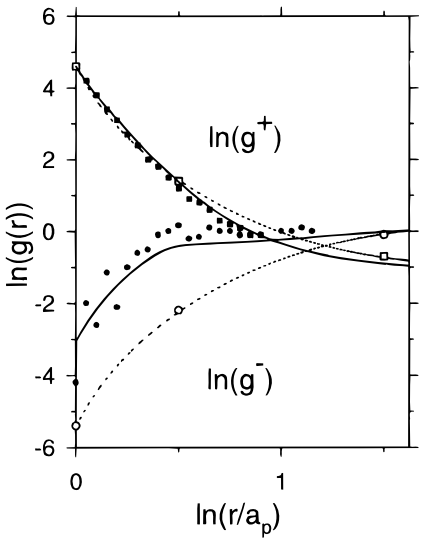

Figure 1. Polyion−simple ion radial distribution functions in the cell containing divalent counterions with $R_c = 65$ Å and salt concentration $c_s = 0.0125$ mol/dm^3: solid lines are results of BBGY; the dotted lines are results of PB; the filled squares and circles are results of MC simulations taken from Figure 13 of ref 19; the open squares and circles are results of PB from Figure 13.

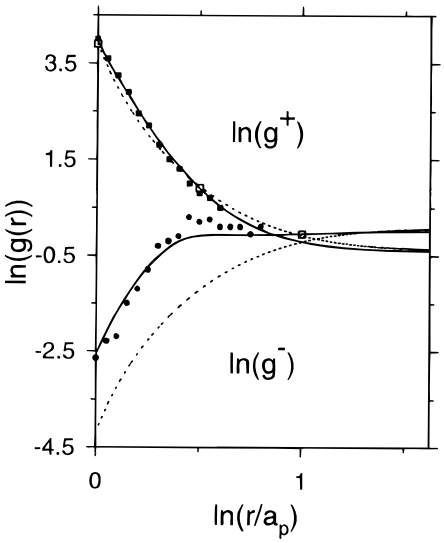

Figure 2. Polyion−simple ion radial distribution functions in the cell containing divalent counterions with $R_c = 65$ Å and salt concentration $c_s = 0.05$ mol/dm^3. Symbols as given in Figure 1; the squares and the circles are taken from Figure 14 of ref 19.

discontinuity. The curves of the mean electrostatic potential ψ are found to be identical in this case (data not shown). We can conclude that the PB equation is a good approximation for 1:1 electrolytes and errors are low even in case of so highly charged macroion as the DNA at strong dielectric discontinuity. A different picture is observed for 2:1 electrolyte which is a more critical test of electrical double-layer theory. Figures 4−8 indicate that not merely the PB theory fails in this case (which is a well-known fact) but the model with uniform permittivity becomes incorrect for divalent ions. The calculations were performed for two salt concentrations: $C = 0.0167$ M (Figures 4 and 5) and $C = 0.167$ M (Figures 6−8). The McMillan−Mayer level of description (the solvent continuum model) is known to be justified for such concentrations in the case of bulk electrolyte.[23] As seen from Figures 4, and 6−8, the influence of dielectric boundaries on ionic distributions is notable within the internal, highly charged region of the double layer (up to 6 Å from the surface of the cylinder). The differences between BBGY curves for $\epsilon = 2$ and for $\epsilon = 80$

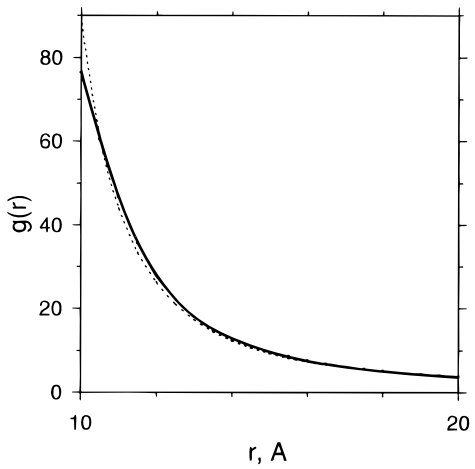

Figure 3. Polyion−counterion radial distribution functions for 1:1 salt at $c_s = 0.05$ M, ion diameter is 4 Å; the solid line is a solution of the BBGY equation for $\epsilon = 2$, $\epsilon_w = 80$; the dotted line is a solution of the PB equation.

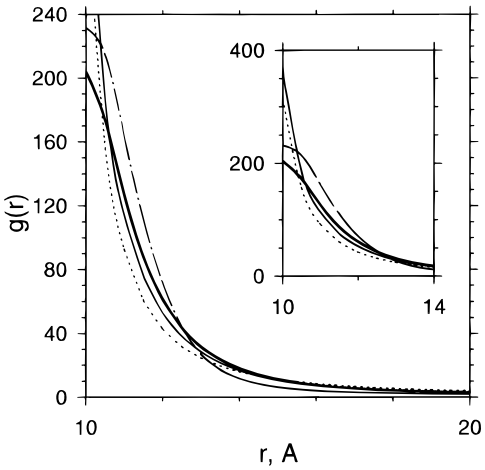

Figure 4. Polyion−counterion radial distribution functions for 2:1 salt at $c_s = 0.0167$ M, ion diameter is 4 Å; the thick solid line corresponds to the BBGY equation for $\epsilon = 2$; the thin solid line corresponds to the BBGY equation for $\epsilon = \epsilon_w = 80$; the thin dash-dotted line represents results for the same parameters as the thick solid curve except for the ion diameter equal to 2 Å; the dotted line is a solution of the PB equation.

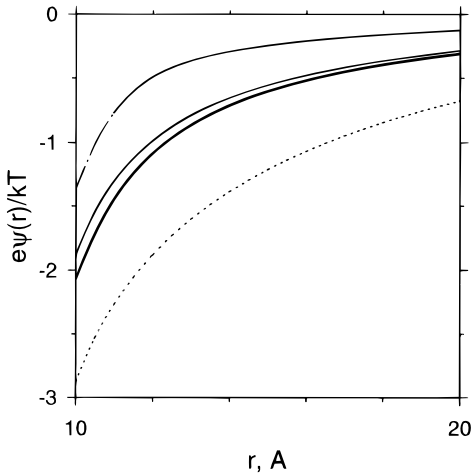

Figure 5. The mean electrostatic potential for data shown in Figure 4. Notation as given in Figure 4.

are comparable to the differences between BBGY curves for $\epsilon = 80$ and solutions of the PB equation in this region. The effect originates from the behavior of the η function at distances 2−6 Å from the surface where the influence of image interactions is

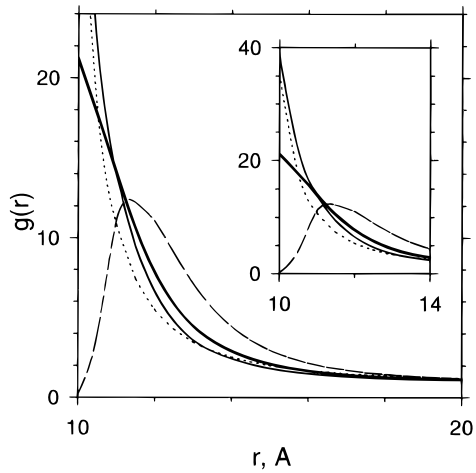

Figure 6. Counterion distribution functions for 2:1 salt at $c_s = 0.167$ M, ion diameter is 4 Å. Notation as given in Figure 4; the dashed line is a solution for dielectric boundary at $r = 9$ Å.

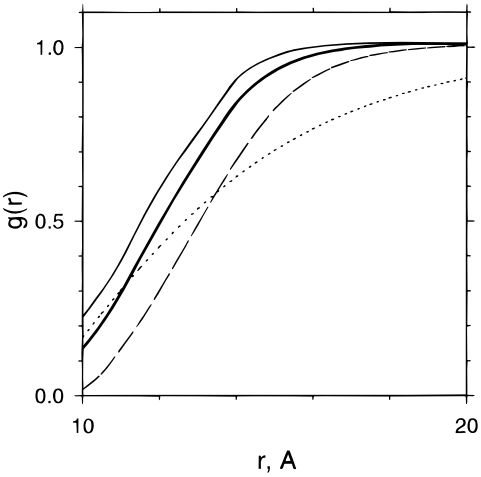

Figure 7. Co-ion distribution functions for 2:1 salt at $c_s = 0.167$ M; ion diameter is 4 Å. Symbols as given in Figure 6.

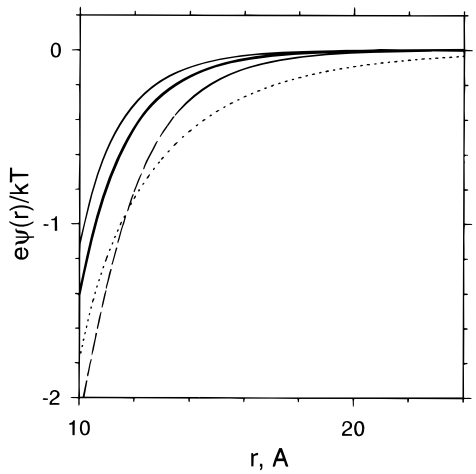

Figure 8. The mean electrostatic potential for 2:1 salt, $c_s = 0.167$ M. Notation as given in Figure 6.

significant. These interactions are negligible for monovalent ions, but notable for divalent ones for which the effect is four times higher. This additional short-acting repulsive force produces an increase of "effective radius" of the polyion which leads to a horizontal shift of curves calculated in the absence of dielectric discontinuity. Starting from higher distances ($r =$ 14 Å), all the curves for $\epsilon = 2$ are, in fact, the same curves for uniform permittivity but shifted about 0.5−1 Å from the dielectric boundary. This can be clearly observed in Figures 5

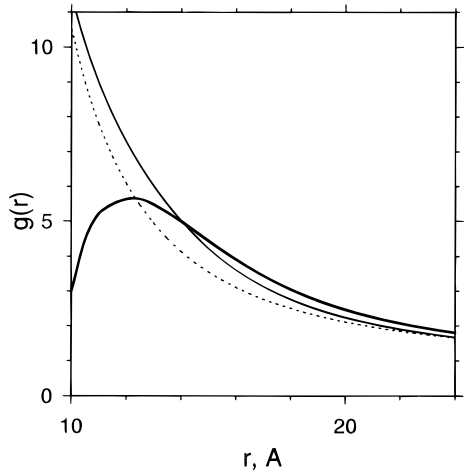

Figure 9. Counterion distribution functions for 2:1 salt, $c_s = 0.0167$ M; ion diameter is 4 Å; charge density of the polyion is one fifth of that of the DNA. The thick solid line corresponds to the BBGY equation for $\epsilon = 2$; the thin solid line corresponds to the BBGY equation for $\epsilon = \epsilon_w = 80$; the dotted line is a solution of the PB equation.

and 8, representing the mean electrostatic potential. Although the shift seems to be low, it obviously depends on the location of the dielectric boundary which was arbitrarily taken at $r = 8$ Å. In other words, the shift of resulting curves depends on a region where a macroscopic description is unphysical. The effect is illustrated in Figures 6−8 where results for the same model with dielectric boundary taken at $r = 9$ Å are included. The observed additional shift of curves is about 1 Å, corresponding to the difference of dielectric boundary locations. We can conclude that at significant separation from the surface the dielectric discontinuities effect is a matter of macromolecule's geometry definition, but it is not so in the vicinity of the macromolecule.

It should be noted that errors of calculations are also reflected in this shift of curves because they mainly originate from errrors of the η function in the closest vicinity of the dielectric boundary. If one increases the grid spacing within $^1/_2$ of its value, the resulting curves remain stable within a few percents except for the dielectric discontinuity model at low ionic concentration ($\epsilon = 2$, $C = 0.0167$ M, Figures 4 and 5). In this case notable instability of the calculated values of $\eta(r)$ (up to 2 times) is observed in the closest vicinity of the cylinder ($r <$ 12 Å) as the grid spacing becomes comparable to the small region of a strong change of $\nabla\eta$. Data in Figures 4 and 5 are given for the grid spacing of 1 Å. The charge−image repulsion obtained in this region at the grid spacing of 1.3 Å is higher, so the thick curve in Figure 5 might be right shifted up to 0.3 Å. A change of the grid size at the fixed grid spacing does not affect results.

The discrepancies between the BBGY and PB equations strongly depend on ionic diameter, as illustrated in Figures 4 and 5 (the ion radius of 1 Å is used for comparison with the radius of hard-core ion−DNA interactions remaining 2 Å.) The choice of macromolecule's internal permittivity is not critical as it follows from high similarity of curves for $\epsilon = 2$ and $\epsilon =$ 10 (data not shown). The influence of dielectric discontinuities on the mean electrostatic potential is not so significant in the closest vicinity of the cylinder as for ionic distribution functions. Even in this region it can be described in terms of the mentioned above shift of curves.

Although the effect of dielectric discontinuities is notable and comparable to the effect of interionic correlations, it is actually suppressed by screening inside the dense double layer due to highly charged nature of the DNA. The last follows from calculations for the same model but for lower charge density of the polyion, which is reflected in Figure 9. The 5 times lower charge density is taken and one can see a significant influence of image interactions on the resulting curves. It is important to note that despite the relatively short-acting nature of image forces (up to 6−8 Å from the dielectric boundary), they essentially affect the chemical potential of the macromolecule due to the osmotic pressure term of free energy.[24] This term always grows at an increase of ionic concentration, which is reflected in thermodynamics of colloids.[21] In particular, it is responsible for the salting-out effect on the protein solubility. We conclude that the dielectric discontinuities should be involved in the description of electrostatic properties of relatively weakly charged macromolecules such as proteins.

The application of numerical realization of the BBGY theory indicates that the method is quite efficient for studying macromolecules−multivalent ions interactions. All effects obtained with the HNC equation and the MC simulations for cylindrical polyion are observed in our results. In particular, one can see the charge reversal (overneutralization of the polyelectrolyte) for 2:1 salt, described in ref 25 (the mean potential changes its sign at $r >$ 18 Å, Figure 8). The method can be developed for more realistic models of macromolecules on the basis of numerical implementation of eq 5 which is quite similar to the nonlinear PB equation. The only disadvantage in comparison with the PB equation is a high cost of computations, but such price has to be paid independently on a method chosen (integral equations, MC simulations, or BBGY equations) if the systems with multivalent ions are to be studied adequately.

References and Notes

(1) deHaseth, P. L.; Lohman, T. M.; Record, M. T., Jr. *Biochemistry* **1977**, *16*, 4783.
(2) Anderson, C.; Record, M. T., Jr. *Biophys. Chem.* **1980**, *11*, 353.
(3) Manning, G. S. *Q. Rev. Biophys.* **1978**, *11*, 179.
(4) Murthy, C. S.; Bacquet, R. J.; Rossky, P. J. *J. Phys. Chem.* **1985**, *89*, 701.
(5) Mills, P.; Anderson, C. F.; Record, M. T., Jr. *J. Phys. Chem.* **1985**, *89*, 3984.
(6) Yayaram, B.; Sharp, K. A.; Honig, B. *Biopolymers* **1989**, *28*, 975.
(7) Klement, R.; Soumpasis, D. M.; Jovin T. M. *Proc. Natl. Acad. Sci. U.S.A.* **1991**, *88*, 4631.
(8) Garcia, A. E.; Soumpasis, D. M. *Proc. Natl. Acad. Sci. U.S.A.* **1989**, *86*, 3160.
(9) Sharp, K. A. *Biopolymers* **1995**, *36*, 245.
(10) Carnie, S.; Torrie, G. M. *Adv. Chem. Phys.* **1984**, *56*, 141.
(11) Kjellander, R.; Marcelja, S. *J. Chem. Phys.* **1985**, *82*, 2122.
(12) Kjellander, R.; Akesson, T.; Jonsson, B.; Marcelja, S. *J. Chem. Phys.* **1992**, *97*, 1424.
(13) Levine, S.; Bell, G. M. *J. Phys. Chem.* **1960**, *64*, 1188.
(14) Bell, G. M.; Levine, S. In *Chemical Physics of Ionic Solutions*; Conway, B. E., Barradas, R. G., Eds.; Wiley: New York, 1966.
(15) Levine, S.; Outhwaite, C. W. *J. Chem. Soc., Faraday Trans. 2* **1978**, *74*, 1670.
(16) Outhwaite, C. W.; Bhuiyan, L. B. *Mol. Phys.* **1991**, *74*, 367.
(17) Outhwaite, C. W. *J. Chem.Soc., Faraday Trans. 2* **1986**, *82*, 789.
(18) Outhwaite, C. W.; Bhuiyan, L. B. *J. Chem. Soc., Faraday Trans. 2* **1983**, *79*, 707.
(19) Das, T.; Bratko, D.; Bhuiyan, L. B.; Outhwaite, C. W. *J. Phys. Chem.* **1995**, *99*, 410.
(20) Bratko, D.; Jonsson, B.; Wennerstrom, H. *Chem. Phys. Lett.* **1986**, *128*, 449.
(21) Arakawa, T.; Timasheff, S. N. *Methods Enzymol.* **1985**, *114*, 49.
(22) Hoye, J. S.; Stell, G. *J. Chem. Phys.* **1995**, *102*, 2841.
(23) Sloth, P.; Sorensen, T. S. *J. Phys. Chem.* **1990**, *94*, 2116.
(24) Sharp, K. A.; Honig, B. *J. Phys. Chem.* **1990**, *94*, 7684.
(25) Montro, J. C. G.; Abascal, J. L. F. *J. Chem. Phys.* **1995**, *103*, 8273.